A Sequence Matching Approach for GNSS-Based Orbit Determination Using Dynamic Time Warping

# A Sequence Matching Approach for GNSS-Based Orbit Determination Using Dynamic Time Warping


Francesco Fiorina
*Dept. of Electronics & Telecommunications (DET)*
*Politecnico di Torino*
Turin, Italy
francesco.fiorina@polito.it

Oliviero Vouch
*DET*
*Politecnico di Torino*
Turin, Italy
oliviero.vouch@polito.it

Andrea Nardin
*DET*
*Politecnico di Torino*
Turin, Italy
andrea.nardin@polito.it

Fabio Dovis
*DET*
*Politecnico di Torino*
Turin, Italy
fabio.dovis@polito.it

Claudia Facchinetti
*Italian Space Agency*
*ASI*
Rome, Italy
claudia.facchinetti@asi.it

Mario Musmeci
*Italian Space Agency*
*ASI*
Rome, Italy
mario.musmeci@asi.it



***Abstract*—Accurate navigation in deep space and lunar environments poses significant challenges due to limited GNSS signal availability and the need for robust state estimation that may take advantage of additional trajectory information. This paper investigates the application of sequence matching (SM) techniques to align a GNSS-based trajectory with a predesigned aiding trajectory (AT), a crucial step in enhancing GNSS-based Position, Navigation, and Timing (PNT) solutions. We formulate the SM problem as a generalized constrained optimization problem and introduce, as a solution, a locally weighted Dynamic Time Warping (DTW) method tailored for GNSS state estimation fusion in challenging environments. The proposed approach is validated through comparisons with an exhaustive search benchmark and extended to assess different local cost functions—based on quasi-norm operators and angular distance—within both classical DTW and the locally weighted DTW framework. Performance analysis, conducted using realistic RF signal simulations for the cislunar environment and trajectories with error-affected sampling rate, demonstrates the effectiveness of the proposed method in handling signal degradation and time misalignment. These findings contribute to advancing autonomous space navigation, reducing reliance on ground-based tracking, and supporting future deep-space missions.**



***Index Terms*—Global Navigation Satellite System, Dynamic Programming, Space communications, Space exploration, Radio Navigation, Time series analysis**


## I. Introduction

The space sector is experiencing significant growth, entering a new golden era where humanity is returning to the Moon and advancing further into space exploration. As this process scales up, the need for accurate and autonomous Orbit Determination (OD) and Position, Velocity, and Time (PVT) estimation of space vehicles is increasing. Currently, spacecraft navigation, positioning, and maneuvering are strongly dependent on ground segment assets. In particular, the OD techniques are based on Direct-to-Earth (DTE) radiometric tracking data from the ground segment facilities [1]. Infrastructures such as National Aeronautics and Space Administration (NASA)'s Deep Space Network (DSN) [2], [3] and European Space Agency (ESA)'s European Space Tracking Network (ESTRACK) collaborate to form a network that provides communication support, telemetry, tracking, command transmission, and data relay to and from spacecraft involved in deep space or interplanetary missions. The observations retrieved from ground-based equipment typically include radiometric data such as Doppler measurements and two-way ranging, as well as angular measurements. These are combined with on-board measurements from systems like gyroscopes, star trackers, and accelerometers to improve spacecraft navigation accuracy. These techniques enable semi-autonomous navigation by providing the OD required for various mission operations. On the other hand, some spacecraft maneuvers are still commanded from the ground, executed via telecommands from Ground Stations (GSs). Although ground-based assets are well established and effective, relying on them for OD management, navigation, positioning, and maneuvering introduces several drawbacks, such as:

*i)* high operational costs;
*ii)* limited ground segment resources;
*iii)* large-scale ground antennas and complex support infrastructure;
*iv)* round-trip and processing delays, which are dangerous for latency-critical operations [4], [5].

In light of the accelerated growth in the domain of space exploration, coupled with the advent of new deep space missions, it becomes crucial to resolve the existing drawbacks promptly. A technology that can be investigated to overcome ground-based assets limitations is precisely Global Navigation Satellite System (GNSS). Although GNSSs are widely used and highly effective on Earth, they were not originally designed for space applications.

An example of how GNSS technology is being explored in high-altitude environments is the Lunar GNSS Receiver

Experiment (LuGRE), a joint NASA-Agenzia Spaziale Italiana (ASI) payload of the Firefly Blue Ghost Mission 1 (BGM1) mission [6]–[8]. This ambitious experiment is the first ever aimed at demonstrating GNSS signal reception beyond 30 Radii Earth (RE) [9] and Position, Navigation, and Timing (PNT) at Moon surface and during the Moon Transfer Orbit (MTO) phase.

Despite the challenges, GNSS remains a well-established and reliable infrastructure, suitable for exploitation in deep space. Over the years, numerous solutions have been proposed in the literature to enhance spacecraft autonomy and improve OD exploiting GNSS. As an example, the Orbital Filter (OF) proposed by Capuano et al. in [10], consists in an Extended Kalman Filter (EKF)-based architecture tailored for MTO. However, the OF may struggle in providing accurate results in certain conditions, especially at higher altitudes due to weak signals and Geometric Dilution Of Precision (GDOP). To overcome those limitations Capuano et al. designed an advanced version of the OF in [11]. Nevertheless, those methods are characterized by a non-negligible computational complexity. They need many a-priori information like Guidance Navigation and Control (GNC) inputs, precise force models accounting for the gravitational effects related to solar system bodies, atmospheric drag, solar radiation pressure and other non negligible contributions. To surmount the needing of a considerable number of a-priori information the Trajectory Aware - Extended Kalman Filter (TA-EKF) technique was designed by Vouch et al. [5]. This EKF architecture exploits GNSS and a set of aiding information about the spacecraft position and velocity states (no clock offset and drift are provided). The aiding information can be generated trough an high precision orbit propagator or can be known from a pre-mission orbit plan (*Aiding Trajectory (AT)*). However, GNSS states and the aiding information are not time aligned. In this context, handling not time aligned sequences presents several obstacles [4], [5].

This work addresses these issues by applying Sequence matching (SM) techniques, especially within the context of the LuGRE project. SM is a crucial preliminary step before integrating the aiding information into an estimation algorithm, such as the TA-EKF.

## II. The Sequence Matching problem and its solution

SM involves finding meaningful matches between two Multi-Dimensional Sequences (MDSs) [12]. MDSs represent the evolution over time of a point in a multidimensional space (also called a *sample*). They can be modeled as matrices in which each row corresponds to a specific time instant and the number of columns is equal to the number of dimensions of the sample. In the context of this work, the two MDSs for which we seek alignment are

- a *GNSS-based trajectory*, i.e. a sequence of GNSS single-point positioning estimates obtained as a Least Mean Square (LMS) regression from ranging observables. This sequence is denoted by the MDS $\mathbf{X} \in \mathbb{R}^{M,L}$ and each sample is of the form:
$$\boldsymbol{x}_m = (x_m, y_m, z_m, \dot{x}_m, \dot{y}_m, \dot{z}_m) \tag{1}$$
- an *aiding trajectory (AT)* that encapsulates a priori information on the spacecraft state, and may refer to a pre-designed trajectory that the spacecraft is intended to follow while traveling. It is associated to $\mathbf{Y} \in \mathbb{R}^{N,L}$ and each sample
$$\boldsymbol{y}_n = (x_n, y_n, z_n, \dot{x}_n, \dot{y}_n, \dot{z}_n) \tag{2}$$
includes the spacecraft position and velocity states at the $n$-th epoch.

Note that $N$ and $M$ are the sequence lengths and $L$ is the sample dimension.

### A. Problem statement

The need to solve the SM problem arises from the requirement to identify samples of $\mathbf{X}$ and $\mathbf{Y}$ that provide the best match while being aligned in time. If two sequences are aligned in time the match is said time-consistent. This is essential for properly integrating the matched samples into state estimation algorithms that can fuse each sample, $\boldsymbol{x}_m$, along with its corresponding aiding samples $\boldsymbol{y}_n$.

Such design requirement can be formulated trough the optimization problem:

$$\mathbf{S}^* = \arg\min_{\mathbf{S}} \; f(\mathbf{X}, \mathbf{Y}, \mathbf{S}) \tag{3a}$$
$$\text{s.t.} \;\; s_{n,m} + s_{d,m+1} - 1 \leq 0 \tag{3b}$$
$$d - n + 1 \leq 0 \tag{3c}$$
$$\mathbf{S}^T \mathbb{1}_{N\times 1} - \mathbb{1}_{M\times 1} = \mathbb{O}_{M\times 1} \tag{3d}$$

where the following quantities have been introduced:

- $\mathbf{S} \in \{0,1\}^{N,M}$ is a binary matrix which records the matches. It can therefore effectively describe a pairwise match between the samples of two sequences. Each entry $s_{n,m}$ is set to 1 when $\boldsymbol{x}_m$ is matched to the aiding sample $\boldsymbol{y}_n$. The optimal match is given by $\mathbf{S}^*$.
- $f(\mathbf{X}, \mathbf{Y}, \mathbf{S})$ is the global cost function. It is used for matching $\mathbf{X}$ and $\mathbf{Y}$ based on a given $\mathbf{S}$-matrix. The global cost function generally depends on a local cost function $c(\boldsymbol{x}_m, \boldsymbol{y}_n)$, which is also regarded as Distance Function (DF). In this context, we adopt as global cost function the accumulated local cost such that
$$f(\mathbf{X}, \mathbf{Y}, \mathbf{S}) = \sum_{n=1}^{N} \sum_{m=1}^{M} c(\boldsymbol{x}_m, \boldsymbol{y}_n) s_{n,m} \tag{4}$$
meaning that the sum is computed considering the DF between the $m^{th}$ sample of $\mathbf{X}$ and $n^{th}$ sample of $\mathbf{Y}$ when $s_{n,m} = 1$.
- $c(\boldsymbol{x}_m, \boldsymbol{y}_n)$ is a DF. It measures the distance between two samples. Some example of DF are the Angular Distance (AD) or the Euclidean Distance (ED), the Manhattan Distance (MD) and the Hamming Distance (HD), which

are three particular cases of the $L_p$ distance ($p = 2, 1, 0$ respectively).

Specifically, $L_p$ distances are related to norms with $p \geq 1$, while *quasi-distance* functions correspond to $0 < p < 1$ and are associated with $L_p$ quasi-norms. Note that the particular case $p = 0$ yields a pseudo-norm, but is a legitimate DF [13]–[16].

Unlike distance functions, quasi-distance functions do not satisfy the triangular inequality. About $L_p$ distances, the literature suggests that certain precautions should be taken depending on the dimensionality of the dataset. In particular, for dimensionality $L \geq 3$, it is recommended to use MD or $L_p$ quasi-norms with $p < 1$. When data are noisy, smaller values of $p$ enhance the contrast between the nearest and furthest points [14]. For the sake of completeness, (5) presents the computation of the local cost using the $L_p$ norm, $L_p$ pseudo-norm and $L_p$ quasi-norm, evaluated between the sample pair $\boldsymbol{x}_m$ and $\boldsymbol{y}_n$, resulting in

$$c(\boldsymbol{x}_m, \boldsymbol{y}_n) = \begin{cases} \left(\sum_{l=1}^{L} |x_{m,l} - y_{n,l}|^p\right)^{\frac{1}{p}}, & p > 0 \\ \sum_{l=1}^{L} \mathbf{1}(x_{m,l} \neq y_{n,l}), & p = 0 \end{cases} \tag{5}$$

where $\mathbf{1}(\cdot)$ is the indicator function that counts the number of nonzero differences.

To effectively solve the optimization problem in (3), so that a solution fits a SM application, it is necessary to take into account a fundamental constraint imposing a *monotonic match*: given a match of $\boldsymbol{x}_m$ with $\boldsymbol{y}_n$, then $\boldsymbol{x}_{m+1}$ can only be matched with aiding samples going from n to N. For example, matching $\boldsymbol{x}_1$ with $\boldsymbol{y}_3$ means that $\boldsymbol{x}_2$ cannot be matched with any $\boldsymbol{y}_n$ having $n < 3$. In other words, SM cannot go back in time. Given $s_{n,m} = 1$ (a match between $\boldsymbol{x}_m$ and $\boldsymbol{y}_n$), all the entries from $s_{1,m+1}$ up to $s_{d,m+1}$ must be 0 (i.e., no matches) (cf. (3b)), where $d$ is an index that can only be less than or equal to $n - 1$ (cf. (3c)).

The *match uniqueness* (i.e., $\boldsymbol{x}_m$ is matched with only one $\boldsymbol{y}_n$) is achieved imposing that each column contains a single 1, hence that each column sums up to 1 (cf. (3d)).

### B. Dynamic Time Warping

Among various SM methods identified in literature (Mono Dimensional Matching Search (MDMS), Correlation, Angular Metric for Shape Similarity (AMSS), Dynamic Time Warping (DTW), Edit distance on Real Penalty (ERP), Edit Distance on Real sequences (EDR) and Longest Common Sub Sequence (LCSS)) [17]–[21], DTW is chosen in this work for its flexibility and ability to handle different sampling frequencies.

DTW is a classical technique for solving SM problems using dynamic programming [17]. It allows one-to-many matches by stretching or compressing sequences, enabling the matching of individual samples. This technique solves an optimization problem similar to (3), but without constraint (3d). Additionally, it includes the following constraints:

$$s_{1,1} = 1, \tag{6a}$$

$$s_{N,M} = 1, \tag{6b}$$

$$s_{n,m} + s_{n+1,m+1} + s_{n+1,m} + s_{n,m+1} = 1, \tag{6c}$$

In particular, the DTW is based on the construction of three matrices:

- The cost matrix $\mathbf{C} \in \mathbb{R}^{N,M}$ contains the costs of matching two samples $\boldsymbol{y}_n$ and $\boldsymbol{x}_m$, and it is build as

$$\mathbf{C} = \begin{bmatrix} c_{1,1} & \cdots & c_{1,M} \\ \vdots & \ddots & \vdots \\ c_{N,1} & \cdots & c_{N,M} \end{bmatrix} \tag{7}$$

  where $c_{n,m} = c(\boldsymbol{y}_n, \boldsymbol{x}_m)$. The cost is computed using a DF, whose choice is arbitrary. Consequently, all the possibilities mentioned in Section II-A can be used.
- The accumulated cost matrix, $\mathbf{G} \in \mathbb{R}^{N,M}$ is built in a dynamic programming fashion from $\mathbf{C}$. Each cell $g_{n,m}$ contains the accumulated cost that one would have to match both the sequences from $\boldsymbol{y}_1$ and $\boldsymbol{x}_1$ up to $\boldsymbol{y}_n$ and $\boldsymbol{x}_m$. It is built in a recursive way:

$$g_{n,m} = \begin{cases} \sum_{i=1}^{n} c_{n,1} \text{ if } m = 1 \\ \sum_{i=1}^{m} c_{1,m} \text{ if } n = 1 \\ c_{n,m} + \min\{g_{n-1,m-1}, g_{n,m-1}, g_{n-1,m}\} \\ \qquad\qquad\qquad\qquad \text{if } m, n > 1 \end{cases} \tag{8}$$

- The direction matrix, $\mathbf{D} \in \mathbb{S}^{N,M}$ with $\mathbb{S} := \{1, 2, 3\}$, defines the optimal matching path. It is built alongside $\mathbf{G}$, and it acts as a map for the best matching path retrieval. Each cell

$$d_{n,m} = \begin{cases} 1 & \text{if } g_{n,m} = c_{n,m} + g_{n-1,m-1} \\ 2 & \text{if } g_{n,m} = c_{n,m} + g_{n,m-1} \\ 3 & \text{if } g_{n,m} = c_{n,m} + g_{n-1,m} \end{cases} \tag{9}$$

  contains the cheapest next step direction (1 is diagonal, 2 is horizontal, 3 is vertical).

The matching path consists of pairs of indices corresponding to the matched samples minimizing the total accumulated cost. The path is obtained by backtracking from $d(M, N)$ to $d(1, 1)$. This procedure can be eventually done on $\boldsymbol{G}$ following the path giving the lower cumulative cost. Moreover, backtracking is used since it is a global optimization method that, with respect to a forward tracking approach, avoids getting stuck in a local minima [18].

Once the path is retrieved, each sample of $\mathbf{Y}$ is associated to a sample of $\mathbf{X}$, and vice-versa. Nevertheless, a final match like this one is not compliant with (3d). In particular, since in this study case $N \geq M$, the DTW would provide a one-to-many match, associating multiple samples of $\mathbf{Y}$ to a single sample of $\mathbf{X}$. Whereas, the objective is to find the best match between two samples, meaning that for each $\boldsymbol{x_m}$, there must

be exactly one associated $\boldsymbol{y_n}$. This ensures that each GNSS-based trajectory sample has a single corresponding aiding sample, allowing the state estimation architectures to correctly process a single pair of matched samples at each epoch.

To address this issue, a post-processing step on the optimal matrix $\mathbf{S}^*$ obtained from the original DTW is necessary. Given $\boldsymbol{x}_m$ and a set of matched $\boldsymbol{y}_n$ it is then considered only the couple characterized by the lowest local cost $c(\boldsymbol{x}_m, \boldsymbol{y}_n)$. In the end, this algorithm provides a MDS $\hat{\mathbf{Y}} \in \mathbb{R}^{M,L}$ containing only the unique samples of $\mathbf{Y}$ associated to the sequence $\mathbf{X}$.

### C. Locally-weighted Dynamic Time Warping

To improve matching accuracy, a novel weighting strategy is introduced. Weights are applied to prioritize areas (for the match retrieval) of the $\mathbf{G}$ matrix where GNSS and AT samples align more closely. The main idea is to use the information on the local distance between the samples, which is enclosed in the Cost matrix $\mathbf{C}$, to refine the original matches. Since the primary goal of DTW is to minimize the overall cost, some matches with minimal local cost may be missed. This occurs because incorporating these matches would extend the matching path, leading to a higher cumulative cost for the optimal $\mathbf{S}^*$. Therefore, to reduce these omissions, a locally weighted accumulated cost matrix $\mathbf{W_G} \in \mathbb{R}^{N,M}$ is derived:

$$\mathbf{W_G} = \mathbf{C}^{\circ\gamma} \odot \mathbf{G} \ . \tag{10}$$

where $\gamma \in \mathbb{R}^+$ is a parameter that can be tuned to have an hard or a soft weighting. The higher $\gamma$ the more the local cost matrix would prevail over $\mathbf{G}$. In (10) is involved the Hadamard product and power, denoted by the symbols $\odot$ and $^\circ$, respectively.

## III. Methodology

The proposed DTW customization is extensively tested and validated on realistic GNSS data coming from the LuGRE QN400-Space GNSS receiver [9]; the latter have been collected during preliminary navigation experiments in a simulation testbed with Hardware In the Loop (HIL). To extract GNSS observables (i.e. pseudorange, pseudorange rates), the receiver's front-end processed Radio Frequency (RF) signals generated from the Spirent GSS9000 simulator powered by the Sprient SimGEN control software [22]. Specifically, Global Positioning System (GPS) signals in both L1 and L5 bands and Galileo signals in E1 and E5 bands were generated. Each data collection includes the pre-designed spacecraft trajectory, which is used to feed the SimGEN software and drive consistent signal generation. This trajectory serves as the basis for $\mathbf{Y}$ (i.e., the AT) after appropriate manipulations designed to challenge the SM algorithm with difficult aiding data, as described hereafter. Additionally, the data collection includes the sequence $\mathbf{X}$, which consists of GNSS single-point estimates derived from ranging observables computed by the receiver. Both trajectories are sequences of states (positions and velocities) represented in the Earth-Centered Earth-Fixed (ECEF) coordinate system and sampled at 1 Hz. Each sample of both sequences is timestamped to Coordinated Universal Time (UTC).

The test validation is performed by comparing the DTW outcomes with the results obtained through an exhaustive search that solves the optimization problem described in (3). Given the low efficiency of this brute-force approach, benchmarking is only possible considering a limited number of trajectory samples; testing longer sequences would end in an unfeasible problem in terms of required time. Having the exhaustive search as a validation benchmark is a fundamental check, enabling a comparison between its optimal solution and the performance of DTW. This allows for an assessment of how much the DTW deviates from an optimal approach like the exhaustive search. Moreover, to provide a comprehensive analysis, various DFs were tested. This approach made it possible to determine which DF is most suitable for different scenarios.

To give generality to the tested scenarios as well as to challenge the SM algorithm some modifications have been enforced on the AT. In particular

- a resampling with sampling frequency $f_s = 2\,\text{Hz}$;
- a temporal misalignment between GNSS measurements epochs and AT.

The resampling is done to study the algorithm performance when the two sequences have a different sample granularity. After defining the new sampling instants the new points are obtained applying Akima interpolation [23].

The temporal misalignment was simulated by adding an error $\varepsilon \sim \mathcal{N}(0, \sigma^2_{\text{time}})$ on the sampling instants (i.e. timestamps) of the resampled AT. A normally distributed offset is therefore summed to each sampling instant resulting in a variable sampling rate. The value of $\sigma_{\text{time}}$ was set as the largest value guaranteeing no overlapping between the $4\sigma_{\text{time}}$ confidence intervals of two consecutive sampling instants. This ensures consecutiveness in time avoiding that $t_k + \varepsilon_k > t_{k+1} + \varepsilon_{k+1}$ with a 99.9937% probability.

To give an example, Fig 1 shows three different normal PDFs corresponding to as many $\sigma_{\text{time}}$. Considering the green Gaussian, it can be noticed that the two consecutive instants have their probability density function that are not intersecting their $4\sigma_{\text{time}}$. Conversely, the blue curves intersect before the $4\sigma_{\text{time}}$ limit.

A block scheme that summarizes the entire methodology is presented in Fig. 2. In particular, the dual use of the pre-designed spacecraft trajectory is highlighted, as it serves both as ground truth for scenario simulation and as a basis for generating the aiding trajectory by resampling with noisy timestamps. In Fig. 2 are also highlighted the position and velocities of the Satellite Vehicles (SVs) in Line of Sight (LOS), necessary to obtain the states of the spacecraft. In the end the two generated sequences $\mathbf{X}$ and $\mathbf{Y}$ are then matched trough the DTW.

To analyze the performances of the DTW, two different datasets have been considered: dataset simulated at an altitude of 17 RE and corresponding to a portion of the MTO; a dataset simulated at 60 RE and located on the Low Lunar Orbit (LLO).

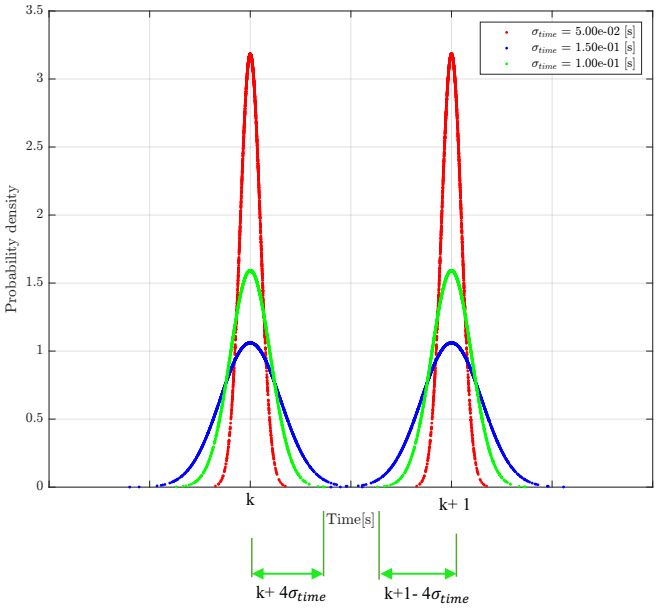


Fig. 1: Probability Density Functions (PDFs) comparison between different $\sigma_{\text{time}}$. The maximum non-overlapping $4\sigma_{\text{time}}$ is chosen through an iterative process with a finite search-step, yielding the desired value. The finite step resolution ensures a conservative result.

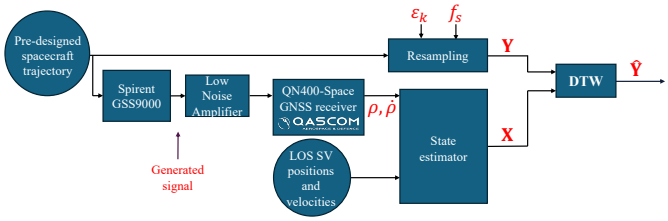


Fig. 2: Block scheme summarizing the adopted methodology

The reason for considering two different altitudes resides in the different contribution of the GDOP. The further the receiver is from the earth and from the GNSS constellations, the worse (higher) will be the GDOP. For this reason, the quality of the PVT single-point solution may degrade, as demonstrated in [24] where a study was conducted on similar datasets. Other than the high GDOP values, a determining factor of PVT estimation performance is RF visibility, which directly affects the number of SVs in LOS.

Each dataset (17RE and 60RE) has been studied in two variants:

- **17RE** and **60RE**: Datasets containing two hours of PVT solutions at 17 RE and 60 RE respectively;
- **EX17RE** and **EX60RE**: Four seconds (i.e. $M = 4$) of PVT solution extracted from the previous datasets. This is done to compare the DTW solution with respect to the one provided by the exhaustive search algorithm, which guarantees optimality. Here are considered smaller chunks of the AT too, in particular $N = 30$.

Each dataset was tested using two case studies: one with time misalignment on AT ($\sigma_{\text{time}} \in \mathbb{R}^+$), referred to as 'noisy timestamp,' and one without time misalignment ($\sigma_{\text{time}} = 0$ s), referred to as 'noiseless timestamp'. For each case study, different DTW configurations were evaluated: the non-weighted DTW (NW), which represents a pure implementation of the classical DTW algorithm, and the locally-weighted DTW (W). Both configurations were applied to the customized DTW algorithm used to solve (3). Tables I and II summarize the conditions under which the DTW experiments were conducted for both phases: validation and testing on the entire dataset respectively.

TABLE I: Experiment settings: Validation

| **Variables** | **Experiments** | | | |
|---|---|---|---|---|
| Dataset | EX 17 RE | | EX 60 RE | |
| $\sigma_{\text{time}}$ $[s]$ | 0 | 0.06 | 0 | 0.06 |
| $f_s$ $[Hz]$ | 2 | 2 | 2 | 2 |

TABLE II: Experiment settings: Testing

| **Variables** | **Experiments** | | | | | | | |
|---|---|---|---|---|---|---|---|---|
| Dataset | 17 RE | | | | 60 RE | | | |
| DTW | NW | | W | | NW | | W | |
| $\sigma_{\text{time}}$ $[s]$ | 0 | 0.06 | 0 | 0.06 | 0 | 0.06 | 0 | 0.06 |
| $f_s$ $[Hz]$ | 2 | 2 | 2 | 2 | 2 | 2 | 2 | 2 |

All the experiments are conducted by comparing the performances of the different DFs mentioned in II-A. Specifically, for each experiment different values of $p$ are evaluated spanning from 0.01 to 30.

The parameter evaluated in the analysis are:

- **Accumulated Time Difference (ATD)**: This metric evaluates the time consistency of the alignment between the samples of the two sequences. Such an evaluation is only possible if both sequences share the same time scale, a fundamental assumption that must be met to assess this parameter. In the experiments, the absolute ATD between pairs of matched samples is analyzed under different DFs, namely AD and $L_p$, while varying $p$.
- **Mismatch**: It quantifies the difference between the exhaustive search and the DTW, it is computed as the number of different matches provided by the two algorithms.

## IV. Results and Discussion

### A. Algorithm's Validation by Exhaustive Search Comparison

*1) EX17RE:* Considering Fig. 3 it is possible to evaluate the variation of the ATD depending on the value of $p$ (cf.(5)). Specifically the different curves are associate to different experiment settings both for validation and testing. In particular, for $p \leq 0.1$, the local weighting does not offer significant benefits. In fact, it performs worse in both noisy timestamp and noiseless timestamp case studies. Concerning the locally

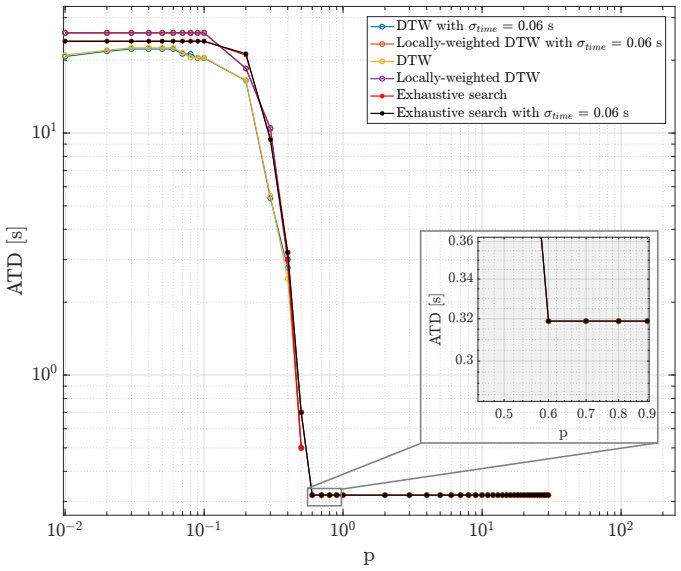


Fig. 3: ATD behavior as a function of $p$ on the EX17RE dataset.

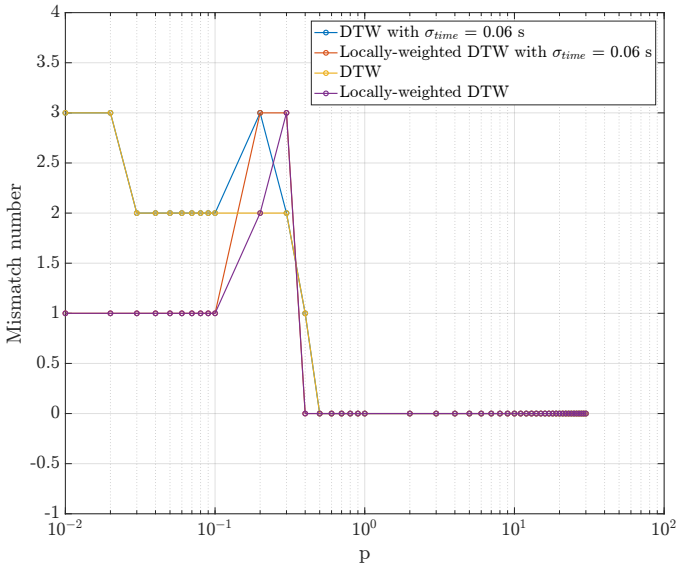


Fig. 4: Sample mismatch between DTW and exhaustive search on the EX17RE dataset.

weighted strategy, a plateau can be observed from $p = 0.01$ up to $p = 0.1$. This behavior is related to the $L_p$ quasi-norms. When the value of $p$ is low, it tends to exaggerate the differences between samples. This, in turn, reduces the resolution with which the distances between samples can be measured. Therefore, the sensitivity of the evaluation is reduced. The lower the $p$, the more the distance function tends to behave like a HD where the distance is 1 if $\boldsymbol{x}_m \neq \boldsymbol{y}_n$ and 0 if $\boldsymbol{x}_m = \boldsymbol{y}_n$. This occurs particularly with the local weighting strategy. The local weighting strategy tends to emphasize the distance between samples, which are then interpreted as "perfectly matching" or "not matching" samples. However, both the non-weighted and the locally-weighted strategies show a drastic drop after $p = 0.1$. This indicates that the $L_p$ distances are starting to provide more realistic and significant information on the distance. This drop in the ATD is associated with a matching process that, in addition to providing well-aligned matches in both position and velocity, offers a good alignment in time. The best result is obtained in the case of experiments performed with the noiseless timestamp datasets. Indeed, it can be seen that for $p \geq 0.6$, the ATD is close to zero, resulting in almost no timing mismatch between the sequences. Similarly, both weighted and non-weighted strategies reach the best result for $p = 0.6$. Nevertheless, since the aiding dataset is moved in time, it is impossible to obtain an ATD equal to 0, as the resampling process introduces an error in the timestamp. At $p = 0.6$, a convergence of the ATD around 0.32s can be observed among all four matched samples. In this case, the local weighting does not show significant improvements. Analyzing the behavior of the exhaustive search, can be noticed that for all values of $p$, the performance in terms of ATD is comparable to that of DTW. In particular, the exhaustive search converges in the same manner as DTW. This result suggests that the DTW algorithm performs effectively in a 17 RE scenario, providing results equivalent to those of the optimal approach. Fig. 4 illustrates the mismatch parameter as a function of the parameter $p$. Each curve corresponds to a different experimental setting. Essentially, each point on a given curve indicates the number of differing matches between the Exhaustive Search and the DTW method for a specific value of $p$. Specifically, for low values of $p$, the local weighting strategy provides a lower mismatch compared to the non-weighted implementation. However, after $p = 0.1$, all the curves begin to behave differently. In particular, only the curve associated with the non-weighted strategy for the noiseless timestamp study case decreases monotonically. Between $p = 0.1$ and $p = 0.3$, several peaks can be observed before all the curves converge to 0 after $p = 0.5$. Like DTW, the exhaustive search provides a solution that varies depending on $p$. Moreover, it should be noted that even if at $p = 0.5$ the two algorithms provide the same match, they both exhibit errors concerning time alignment, as the ATD only converges after $p = 0.6$. Furthermore, it can be observed that the locally-weighted DTW begins to exhibit the same behavior of the exhaustive search at earlier values of $p$, compared to the non-weighted version.

After examining this validation scenario, it can be concluded that, although DTW does not provide the same results as the exhaustive search for all values of $p$, it proves to be a reliable solution for specific values of $p$. Therefore, DTW can be used to match the entire trajectory at 17 RE by exploiting $L_p$ distances with $p \geq 0.6$, where the ATD has converged and no mismatch is observed compared to the benchmark.

*2) EX60RE:* Analyzing Fig. 5, it can be observed that the noiseless timestamp curves of the ATD associated with the DTW converge to the same value for $p \geq 16$. In particular, the non-weighted DTW converges before ($p = 11$). However, in this more challenging environment at 60 RE, DTW cannot

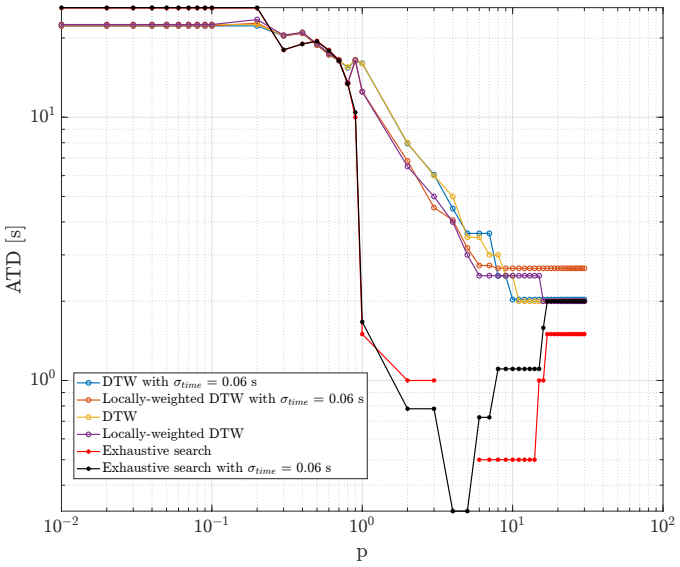


Fig. 5: ATD behavior as a function of $p$ on the EX60RE dataset.

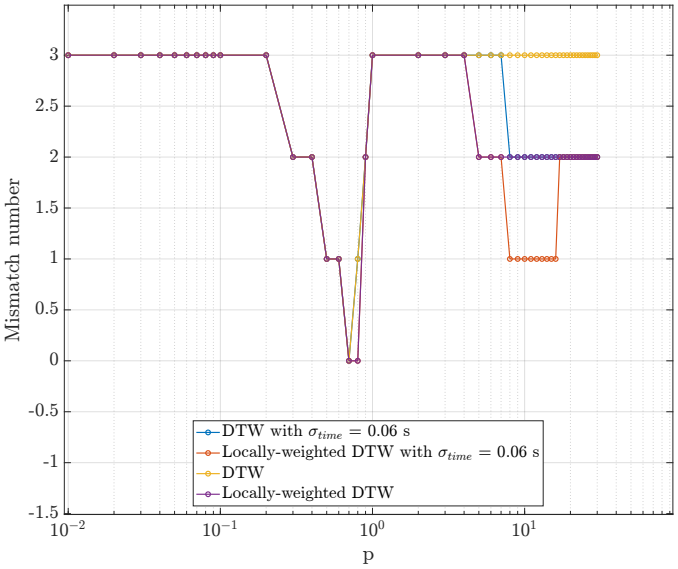


Fig. 6: Sample mismatch between DTW and exhaustive search on the EX60RE dataset.

achieve the same minimum as the exhaustive search. Specifically, the exhaustive search is able to provide a match with an ATD = 0 s for $p = 4$ and $p = 5$ in the noiseless timestamp case, and reaches a minimum ATD for the same values of $p$ in the noisy timestamp case. In this case, the locally-weighted strategy applied on scenarios affected by $\sigma_{\text{time}}$ is showing an under-performing behavior. The locally-weighted strategy converges at a higher $p$ value in the noiseless timestamp case and matches the behavior of the exhaustive search. However, although the DTW matches the benchmark, it does not achieve the optimal result obtained by the exhaustive search. Concerning the non-weighted DTW, it outperforms the locally-weighted strategy in the noisy timestamp case, as it converges to a lower ATD. In Fig. 6, it is possible to see that for $p = 0.7$ all the scenarios present a DTW solution that is equal to the one of the exhaustive search since there is no mismatch. However, at $p = 0.7$, the ATD is greater than 10 seconds. This means that neither the exhaustive search can provide a good time alignment for this specific value of $p$. As the DTW is applied to a more challenging scenario, such as 60 RE, it cannot fully match the exhaustive search and thus becomes sub-optimal. To overcome this inconvenient it may be necessary to increase the weighting order $\gamma$, however, this is not explored in this work. Nevertheless, even though DTW is not coherent with the benchmark, it remains a reliable solution for matching the entire trajectory.

### *B. Norm and Quasi-norm Functions Performance*

*1) 17RE:* After the proposed method's validation through the comparison with exhaustive search, an extended portion of trajectory is analyzed, therefore ingesting a larger number of samples. Considering the ATD in Fig. 7, a key observation is the significant difference between the non-weighted and locally-weighted methods for $0.01 \leq p \leq 0.5$. For these values of $p$, the non-weighted and weighted strategies differ greatly, with the weighted strategy being two orders of magnitude higher. The most interesting behavior occurs around $p = 0.5$, where the noisy timestamp case begins to converge and nearly overlap. However, the non-weighted strategy proves to be more advantageous: the best ATD is achieved with the non-weighted DTW at $p = 0.9$, where it is 0.35% lower than the locally-weighted approach. The superiority of the non-weighted technique is even more evident for the noiseless timestamp study case. Here, the convergence of the curves occurs later, particularly at $p = 1$. After this drop, the two curves start converging but do not overlap. The level of precision in terms of time alignment is thus higher for the non-weighted DTW approach, with the best result being achieved at $p = 1$. After this point, the curve rises again.

The behavior of the timestamp difference between matched samples over time is shown in Fig. 8, which depicts the time difference between the two matched samples at each epoch. The two red stripes represent the $\pm 4\sigma_{\text{time}}$ acceptable range mentioned in Section III and introduced in resampling. In particular, it is depicted the non-weighted version considering the $L_p$ distance giving the best ATD in the noisy-timestamp case. What can be observed is that the errors in time are within the $\pm 4\sigma_{\text{time}}$. The only exception is at the beginning, where there are large oscillations that extend beyond the $\pm 4\sigma_{\text{time}}$ band. However, after 27 seconds, the time differences settle within the two bands, except for an outlier occurring around 20:29.

Fig. 9 depicts the result of the SM. Each box highlights the matches across different dimensions, specifically emphasizing the GNSS-based trajectory $\mathbf{X}$, the matched aiding trajectory $\hat{\mathbf{Y}}$, and the aiding trajectory $\mathbf{Y}$. By examining the states in Fig. 9, it is possible to draw more detailed conclusions regarding the behavior described by the timestamp difference. The

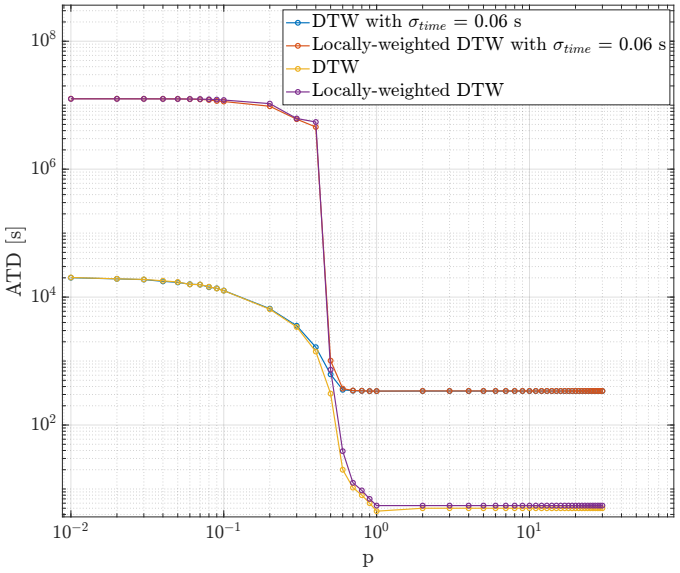


Fig. 7: ATD behavior as a function of $p$ on the 17RE dataset.

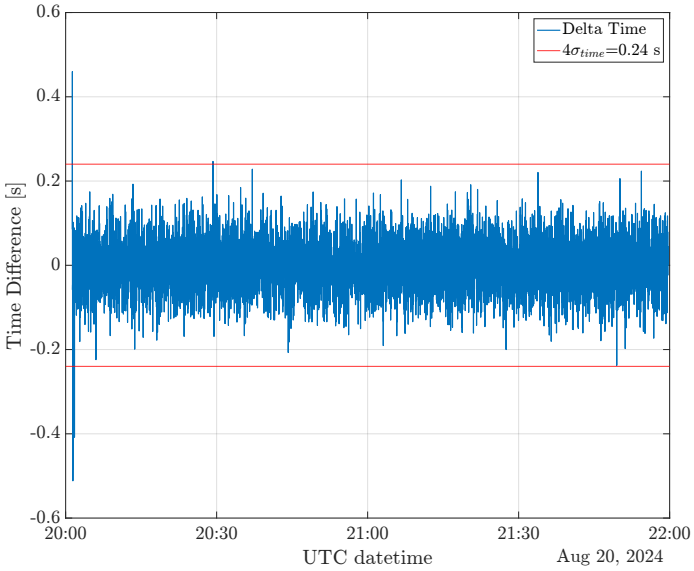


Fig. 8: Time Difference for the non-weighted strategy in the noisy timestamp study case with $p = 0.9$ on the 17 RE dataset.

initial oscillations can be associated with the large variations at the beginning of the trajectories concerning the velocities. This behavior is not surprising, as the DTW algorithm performed as expected, attempting to match the samples that minimize the overall accumulated cost, even if this is not the best choice in terms of local distance. Overall, the situation is somewhat more challenging for the locally-weighted strategy, where the time error is slightly higher during the initial matches. However, after 27 s, it stabilizes and remains within the $\pm 4\sigma_{\text{time}}$ band, with only one outlier.

In Fig. 9 the matching result of the local weighting in the noiseless timestamp case study is depicted (no significant differences compared to the non-weighted DTW can be observed

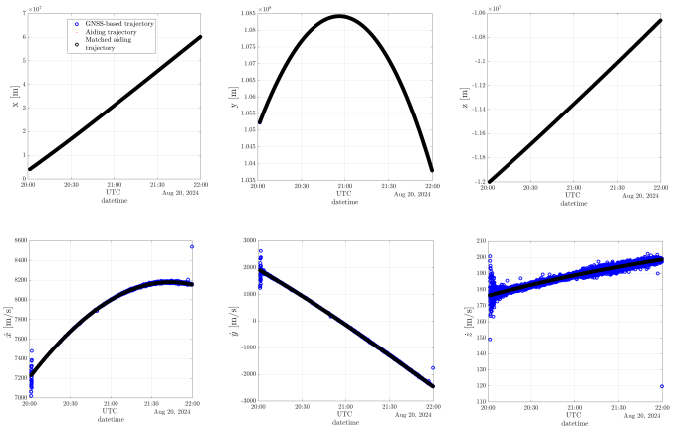

Fig. 9: Matched states for the 17RE dataset using the non-weighted strategy and $p = 1$.

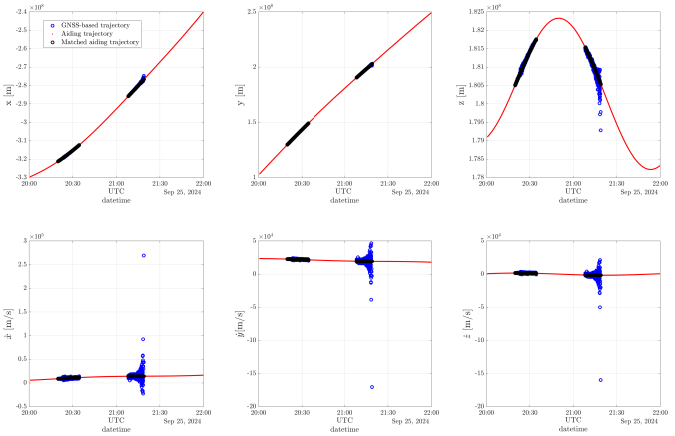

Fig. 10: Matched states for the 60RE dataset using the locally-weighted strategy and $p = 10$.

in terms of matched states). This analysis further restricts the selection of the $L_p$ distance, setting the choice to $L_p$ with $p = 1$ (i.e. MD). Although literature suggests $p < 1$ for $L \geq 3$, this solution represents the best choice for obtaining a minimum ATD in all four scenarios.

*2) 60RE:* This dataset under analysis focuses on the performances of the DTW algorithm working with GNSS states retrieved at 60 RE, which is a more challenging environment compared to 17 RE. In this scenario, a poor GDOP is present because of the unfavorable geometry seen from the moon. Moreover, due to the Earth's occultation the number of available pseudoranges to be used in the multi-lateration problem is reduced. In this case, the GDOP reaches an order of magnitude of $10^6$ [24], making the 60 RE a very difficult scenario for PNT. The moment when poor GDOP occurs in this specific dataset is visible in Fig. 10. In particular, it is evident that the solution precision provided by the GNSS receiver deteriorates until no solution is provided when the number of SV in LOS becomes less than 4. This is more pronounced in the velocities and the z-coordinate, especially in the last matched solution chunk, between 21:08 and 21:20 on 25.09.2024.

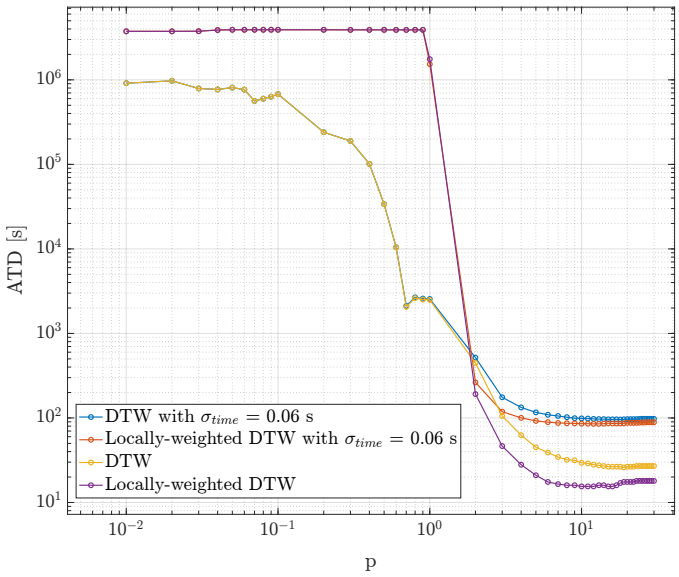


Fig. 11: ATD behavior as a function of $p$ on the 60RE dataset.

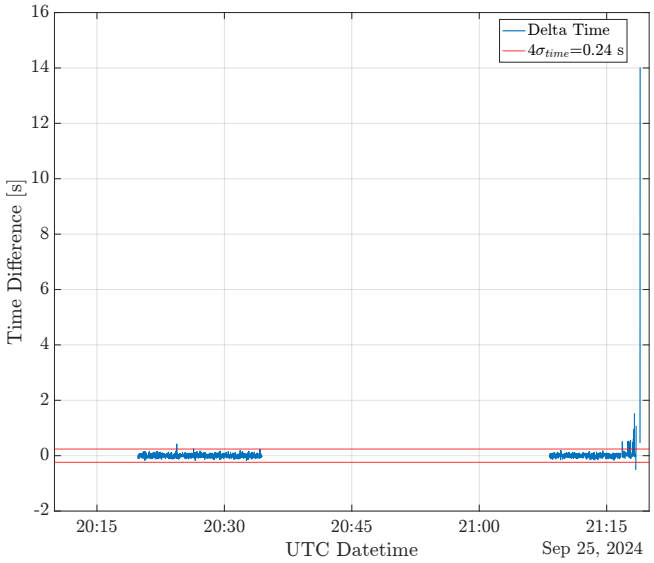


Fig. 12: Time Difference for the non-weighted strategy in the noisy timestamp study case with p=18 on the 60RE dataset

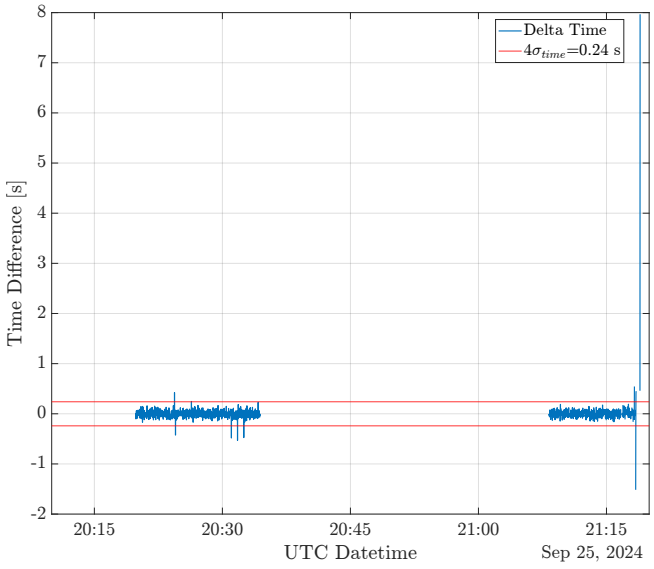


Fig. 13: Time Difference for the locally-weighted strategy in the noisy timestamp study case with p=18 on the 60RE dataset p=12

Considering an extended quantity of information, the trends shown in Fig. 5 are difficult to be detected in the ATD of this dataset (see Fig. 11). However, analyzing the behavior of the ATD in Fig. 11, the local weighting strategy, applied in high GDOP conditions, shows a surprising behavior. It provides a better time alignment than the non-weighted DTW version. Specifically, the ATD for $p = 10, 11, 12$ is 32.26% smaller than the minimum ATD given by the non-weighted DTW strategy for $p = 19$, which is its best result. However, after reaching a minimum for $L_p$ with $p = 19$, the curve associated with the non-weighted implementation starts to increase again.

Another interesting observation is that at lunar distances such as this scenario, given the harsh conditions, the convergence of the ATD curve happens for higher values of $p$. For smaller values of $p$, the locally-weighted strategy underperforms compared to the non-weighted DTW strategy. The locally-weighted strategy shows a significant drop after $L_p$ with $p = 1$. This is because such a method, when combined with the behavior of the norm for $p < 1$, exaggerates the differences before reaching $L_1$. On the other hand, the non-weighted strategy has a smoother descent. Observing the results obtained from the dataset affected by the time error, the weighting strategy also outperforms the non-weighted DTW. The analysis of the time difference behavior (depicted in Fig. 12 and Fig. 13) reveals that the improvement over other scenarios comes from the last part of the solution. When the GDOP increases, the local weighting reduces the time misalignment. On the other hand, the local weighting may cause some unwanted matches when the GDOP is lower, as seen in the first chunk of Fig. 13, where the outliers number rises from 1 to 5. This also explains why, at 17 RE, the locally-weighted strategies are not the best option. This analysis shows that the locally-weighted strategy is useful only in really critical conditions. Nevertheless, at lunar distances, for trajectory points that are not significantly affected by high GDOP, the non-weighted DTW strategy may require higher values of $p$ compared to shorter distances (e.g., at 17 RE). This can be associated to the higher error in the single-point solution with respect to the MTO scenario. In such cases, good choices could be $p = 18$ or $p = 19$ (cf. Fig. 12).

### C. Angular Distance Performance

As expected, the performance of the AD is comparable to that of the ED. Since AD works similarly to ED, only a single result for the 60 RE scenario is presented.

Fig. 14 represents the variation of ATD as a function of $\sigma_{\text{time}}$ introduced in the resampling process. The different colors in

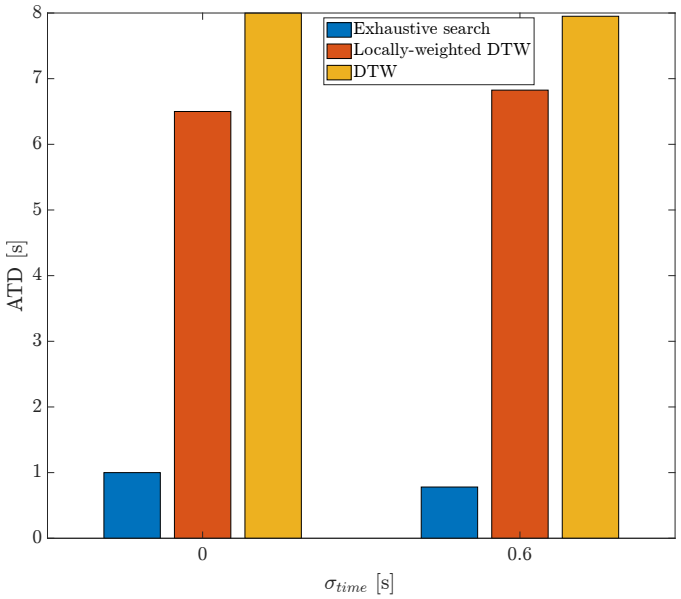


Fig. 14: AD validation comparing DTW to the exhaustive search at 60 RE.

the color bar correspond to specific techniques. In Fig. 14, it is evident that the AD exhibits significantly worse ATD performance compared to the exhaustive search. This suggests that AD is not a suitable choice in terms of DF.

When the AD is applied to the entire 60RE dataset, can be noticed that the ATD values are comparable to those of the ED (see $p = 2$ in Fig. 11). The findings on the AD tests are summarized in Table III. The experiment settings are the same of those in Table II,, particularly for the 60 RE dataset.

| **Experiments results** | | | | |
|---|---|---|---|---|
| ATD $[s]$ | 446 | 517.068 | 191.5 | 263.54 |

TABLE III: AD performances in terms of ATD

## V. Conclusion

The problem of aligning the GNSS single-point solution with the pre-designed AT represents a novel area of application for SM techniques. The harsh conditions in MTO and LLO, characterized by degrading geometric scenarios and GNSS solution unavailability, make this challenge even more complex. This work demonstrated the effectiveness of DTW in addressing this challenge, particularly through the introduction of an original customization and a novel local weighting strategy.

The experimentation revealed that there is no single optimal choice for $p$. Instead, depending on the tested scenario and altitude, more appropriate choices for $p$ were observed.

At a distance of 17RE from the Earth center, the geometric conditions can still be considered acceptable, with a contained value of GDOP. As a result the GNSS solution does not exhibit significant errors. In this scenario, the best choice for $p$ is 1 since it provides the lowest ATD. Furthermore, the proposed locally-weighted strategy does not provide any significant advantages. Under good visibility and acceptable geometry, the customized non-weighted DTW performs effectively.

As the spacecraft reaches lunar altitudes at 60RE, GDOP increases. When the geometric conditions worsen, GNSS-based state estimation becomes less accurate, which can mislead the matching algorithm. In this case, the proposed locally-weighted strategy provides significant beneficial contribution that enhances the robustness of DTW. Notably, when GDOP increases, higher values of $p$ are necessary to yield lower ATD. In particular, the best performance was obtained for $10 \leq p \leq 12$.

The study of SM techniques, particularly the customized DTW, highlights this research's potential to extend GNSS applications to deep space and lunar environments.

## VI. Further Works

During the development of this work, the need to assess the potential benefits of this technique in a state estimation process, particularly in terms of position accuracy became evident. Specifically, such an evaluation could be performed by integrating the method into a Bayesian estimator like the TA-EKF, which is an optimal filter that does not introduce unwanted effects. However, this type of assessment falls outside the scope of the current work and is left as a direction for future investigations.

Other future developments that could further enhance the effectiveness of this technique include:

- **Exploring Different Weighting Orders:** In this study, the local weighting strategy was tested with $\gamma = 1$. Future work could investigate the use of higher weighting orders to improve matching performance in more challenging geometric conditions.
- **Exploring the Observation Domain:** While this research focused on solving a SM problem between sequences whose samples are derived from LMS estimates, future studies could explore the application of the proposed customized DTW to sequences with samples based on GNSS observables. This approach may offer additional flexibility and new insights for space navigation applications.

## Acknowledgment

This study was funded within the contract n. 2021-26-HH.0 ASI/Politecnico di Torino "Attività di R&S inerente alla Navigazione GNSS nello Space volume Terra/Luna nell'ambito del Lunar GNSS Receiver Experiment". The authors would like to thank Qascom and NASA for supplying the representative datasets of LuGRE operations that supported this study.

## References

[1] L. Iess, M. Di Benedetto, N. James, M. Mercolino, L. Simone, and P. Tortora, "Astra: Interdisciplinary study on enhancement of the end-to-end accuracy for spacecraft tracking techniques," *Acta Astronautica*, vol. 94, no. 2, pp. 699–707, 2014. [Online]. Available: https://www.sciencedirect.com/science/article/pii/S0094576513002014

[2] NASA, "What is the Deep Space Network?" 2024. [Online]. Available: https://www.nasa.gov/directorates/somd/space-communications-navigation-program/what-is-the-deep-space-network/#hds-sidebar-nav-4

[3] H. H. Means, "The Deep Space Network: Overburdened and underfunded," *Physics Today*, vol. 76, no. 12, pp. 22–23, 2023.

[4] O. Vouch, A. Nardin, A. Minetto, S. Zocca, F. Dovis, L. Konitzer, J. Joel Parker, B. Ashman, F. Bernardi, S. Tedesco, and S. Fantinato, "Bayesian Integration for Deep-Space Navigation with GNSS Signals," in *2024 27th International Conference on Information Fusion (FUSION)*, 2024, pp. 1–8.

[5] O. Vouch, A. Nardin, A. Minetto, S. Zocca, M. Valvano, and F. Dovis, "Aided Kalman Filter Models for GNSS-Based Space Navigation," *IEEE Journal of Radio Frequency Identification*, vol. 8, pp. 535–546, 2024.

[6] J. J. K. Parker, F. Dovis, B. Anderson, L. Ansalone, B. Ashman, F. H. Bauer, G. D'Amore, C. Facchinetti, S. Fantinato, G. Impresario, S. A. McKim, E. Miotti, J. J. Miller, M. Musmeci, O. Pozzobon, L. Schlenker, A. Tuozzi, and L. Valencia, "The Lunar GNSS Receiver Experiment (LuGRE)," in *Proceedings of the ION ITM 2022 Conference*, NASA and Italian Space Agency (ASI). Long Beach, California: Institute of Navigation, 2022. [Online]. Available: https://ntrs.nasa.gov/api/citations/20220002074/downloads/LuGRE_ION-ITM_2022_Draft8_Submitted_ConferenceProceedings.pdf

[7] K. Schauer. (2023, 3) NASA Delivers Hardware for Commercial Lunar Payload Mission. NASA. Accessed: 2024-09-21. [Online]. Available: https://www.nasa.gov/missions/artemis/clps/nasa-delivers-hardware-for-commercial-lunar-payload-mission/

[8] L. Konitzer, J. J. Parker, B. Ashman, N. Esantsi, C. Facchinetti, F. Dovis, A. Minetto, A. Nardin, F. Bauer, L. Ansalone, and et al., "Science Objectives and Investigations for the Lunar GNSS Receiver Experiment (LuGRE)," in *Proceedings of the 37th International Technical Meeting of the Satellite Division of The Institute of Navigation (ION GNSS+ 2024)*, Sep 2024. [Online]. Available: https://doi.org/10.33012/2024.19711

[9] F. Dovis, A. Nardin, A. Minetto, C. Facchinetti, M. Musmeci, G. Varacalli, J. J. K. Parker, L. Konitzer, S. Sanathanamurthy, L. Valencia, J. J. Miller, F. H. Bauer, S. Fantinato, E. Miotti, M. Boschiero, M. Pulliero, S. Tedesco, F. Bernardi, and S. Guzzi, "Assessing the Usability of GNSS on The Way To The Moon: Getting The LUGRE Payload Ready To Fly," in *Proceedings of the 74th International Astronautical Congress (IAC)*. Baku, Azerbaijan: International Astronautical Federation (IAF), 10 2023.

[10] V. Capuano, F. Basile, C. Botteron, and P.-A. Farine, "GNSS-based Orbital Filter for Earth Moon Transfer Orbits," *The Journal of Navigation*, vol. 69, no. 4, pp. 745–764, 2016. [Online]. Available: https://doi.org/10.1017/S0373463315000843

[11] V. Capuano, E. Shehaj, C. Botteron, P. Blunt, and P.-A. Farine, "An Adaptive GNSS-based Reduced Dynamic Approach for Real Time Autonomous Navigation from the Earth to the Moon," in *Proceedings of the Pacific PNT 2017 Conference*. Honolulu, Hawaii: ION, 5 2017.

[12] H. Wang, Z. Lin, S. McClean, and J. Liu, "Measuring Similarity for Multidimensional Sequences," in *2010 IEEE International Conference on Data Mining Workshops*, 2010, pp. 281–287.

[13] W. Rudin, *Functional Analysis*, 2nd ed. New York: McGraw-Hill, 1991.

[14] C. C. Aggarwal, A. Hinneburg, and D. A. Keim, "On the Surprising Behavior of Distance Metrics in High Dimensional Space," in *Proceedings of the 8th International Conference on Database Theory (ICDT 2001)*, ser. Lecture Notes in Computer Science, vol. 1973. Berlin, Heidelberg: Springer-Verlag, 2001, pp. 420–434. [Online]. Available: https://doi.org/10.1007/3-540-44503-X_27

[15] S. Boyd and L. Vandenberghe, *Convex Optimization*. Cambridge, UK: Cambridge University Press, 2004, section A.1.3 - Examples of norms, including Euclidean and Manhattan distances.

[16] A. Le Franc, J.-P. Chancelier, and M. De Lara, "The Capra-subdifferential of the l0 pseudonorm," 2021, preprint submitted on 30 Dec 2021 (v1), last revised 25 Jan 2023 (v3).

[17] H. Sakoe and S. Chiba, "Dynamic Programming Algorithm Optimization for Spoken Word Recognition," *IEEE Transactions on Acoustics, Speech, and Signal Processing*, vol. 26, no. 1, pp. 43–49, 1978.

[18] M. Müller, *Information Retrieval for Music and Motion*. Berlin, Heidelberg: Springer-Verlag Berlin Heidelberg, 2007, with 136 Figures, 41 in color and 26 Tables.

[19] M. Vlachos, G. Kollios, and D. Gunopulos, "Discovering Similar Multidimensional Trajectories," in *Proceedings of the 18th International Conference on Data Engineering*. IEEE, 2002, pp. 673–684.

[20] L. Chen, M. T. Özsu, and V. Oria, "Robust and Fast Similarity Search for Moving Object Trajectories," in *Proceedings of the 2005 ACM SIGMOD International Conference on Management of Data*. ACM, 2005, pp. 491–502.

[21] L. Chen and R. T. Ng, "On The Marriage of Lp-norms and Edit Distance," in *Proceedings of the 30th VLDB Conference*. Toronto, Canada: VLDB Endowment, 2004.

[22] Spirent, "GSS9000 GNSS Simulator," Spirent Communications, Crawley, UK, 2015.

[23] H. Akima, "A Method of Bivariate Interpolation and Smooth Surface Fitting Based on Local Procedures," *Communications of the ACM*, vol. 17, no. 1, pp. 18–20, 1974.

[24] O. Vouch, A. Nardin, A. Minetto, S. Zocca, F. Dovis, L. Konitzer, J. J. K. Parker, B. Ashman, F. Bernardi, S. Tedesco, and S. Fantinato, "Advancing Autonomous Navigation: Near-Moon GNSS-based Orbit Determination," in *Proceedings of the 37th International Technical Meeting of the Satellite Division of The Institute of Navigation (ION GNSS+ 2024)*, Baltimore, Maryland, USA, September 16–20 2024.